J. Condensed Matter Nucl. Sci. 39 (2025) 210–219

Research Article

Photon Radiation Calorimetry for Anomalous Heat Generation in NiCu Multilayer Thin Film During Hydrogen Gas Desorption

J. Kasagi, T. Itoh, and Y. Iwamura

Research Center for Electron Photon Science, Tohoku University, 982-0826 Japan

Y. Shibasaki, T. Takahashi, and S. Yamauchi

Clean Planet Inc., 105-0022 Japan

Abstract

In order to investigate the anomalous heat effect (AHE) in NiCu multilayer thin films, photon radiation calorimetry has been developed. Three types of photon detectors are employed to cover a wide range of wavelengths from 0.3 μm to 5.5 μm, i.e., photon energies from 0.22 to 4.13 eV. In the present work, the usefulness of the calorimetry is demonstrated for excess heat measurements with samples of pure Ni, NiCu composite layers, and a Cu mono-layer deposited on a Ni substrate. Direct comparisons of photon radiation spectra with and without H_2 easily showed sample-specific differences in excess heat power. The samples of the NiCu composite layer produced larger excess heat. By incorporating the measured radiant power into a heat flow model, the excess heat was deduced to be 4 to 6 W. The energy generated in 80 hours reached 460 $\pm$ 120 kJ: the generated energy per hydrogen atom was at least 410 $\pm$ 108 keV/H atom. This is definitely not a chemical reaction; it produces energy at the level of nuclear reactions.
 ISSN 2227-3123

Keywords: Photon radiation calorimetry, Anomalous heat generation, NiCu multilayer film, H2 gas, Vacuuming - heating

1. Introduction

After the announcement of "Cold Fusion" by Fleischmann and Pons [1], Ni-based metal + H_2 systems were widely studied with electrolysis [2–4], as well as by H_2 gas loading [5–7]. However, in experiments using H_2 gas that attempted to reproduce high-power production in high-temperature conditions, large excess power as reported was not observed. It was reported in measurements by Levi et al. [7], but Valat *et al.* pointed out that they overestimated excess heat by at least one order of magnitude due to errors in emissivity [8]. Budko and Korshunov performed calorimetric measurements in a small experimental setup but no excess heat was observed [9]. In the Google project, Berlinguette *et al.* showed that excess power productions was not observed for 420 measurements under the conditions of high temperature and high H_2 gas pressure with Ni powder including $LiAlH_4$ [10].

On the other hand, in experiments focused on metal nanostructures, Arata and Zhang found that nanosized Pd particles (about 10 nm) with D_2 gas generated greater excess heat [11]. Subsequently, Kitamura *et al.* confirmed

 ISSN 2227-3123

this result using a flow calorimeter: anomalous large heat production was observed not only with D_2 gas but also H_2 gas [12]. Furthermore, they expanded the sample from pure Pd nanoparticles to NiPd composite nanoparticles, and also extended the measurement temperature from room temperature to about 600 K [13]. In a series of experiments performed as an NEDO (New Energy and Industrial Development Organization) project, notable results were obtained as follows: excess power which cannot be explained by chemical reaction was observed up to 600 K not only in the PdNi-D_2 system but also in the PdNi-H_2 system and CuNi-H_2 system [14,15].

We have extended the measurement to much higher temperatures up to 1100 K using nanostructured metal films, instead of the composite amorphous metal powder employed in the NEDO project. The method is rather simple: a nanostructured NiCu multilayer film containing absorbed hydrogen is heated to a high temperature (about 1100 K) and evacuated in a vacuum [16,17]. The measurements were performed at a vacuum level of 10^{-4} Pa or less, and thus the mean free path of the residual gas in the vacuum is more than 10 m, 100 times the inner diameter of the chamber. Therefore, the heat flow from the sample can be ignored except for thermal radiation and a slight conductive heat flow.

To better evaluate excess thermal power, we have explored calorimetry by measuring photons emitted from samples [17]. The objective of the present work is to establish photon radiation calorimetry to obtain solid evidence that anomalous large heat production does occur in the nanostructured NiCu multilayer film during desorption of hydrogen gas, and to evaluate the amount of generated heat at high temperatures with high reliability.

2. Experiment

2.1. Experimental Setup

Figure 1(a) briefly shows a top view of the experimental apparatus showing the inside of the vacuum chamber. Two thin film samples attached to both sides of a ceramic heater, suspended from the lid of the vacuum chamber, are heated up to about 1100 K. Radiant power emitted from the sample surface is measured over a wide range of photon energies with three different detectors covering three different energy ranges. To measure radiation from both sides of the sample, two detectors are required for each energy range. Except for the mid-IR range, there is only one detector for respective range, so measurements for the other side are made by switching the entrance port for those detectors. The data acquired in each detector are combined into one spectrum. This enables not only direct comparison of the radiant power with and without hydrogen, but also reliable evaluation of the excess heat.

Figure 1(b) shows schematically the sample holder. The sample is a thin foil about 0.2-mm thick. A foil is placed on each side of a ceramic heater (made of alumina, $25 \times 25 \times 2.5$ mm^3) which has an R-type thermocouple in the center. The foils are labeled A and B. A 0.3-mm thick insulating plate (Photoveel) is sandwiched between the substrate of the foil and the ceramic heater. The power line of the heater and the thermocouple lead are connected to the outside via hermetic seals. The foils are covered with two Photoveel plates (40×40 mm^2 in area with a hole of 20 mmϕ) and fixed to the frame. Photon radiations from the sample foils are measured by three detectors placed outside the windows of the vacuum chamber, as shown in Fig. 1(a). For mid-infrared region, two sets of TMHK-CLE1350 (which we designate Md-IR detector; effective range 0.22–0.40 eV) are set 40 cm from the sample through long vacuum pipes and BaF_2 windows. In this experiment, Md-IR is used not as a thermometer, but as a radiation power detector measuring the average radiant power in the 0.22–0.4 eV region.

The other two detectors measure the light passing through a quartz window installed in the opposite direction of the long vacuum tube. Behind the quartz window, which is covered with Al foil with a hole of 10 mmϕ on the inner and outer surfaces, the light is focused into an optical fiber cable and then carried by two cables through a splitter. Detectors use an FTIR spectrometer in the near-infrared region, Hamamatsu C15511-01 (which we designate Nr-IR detector; effective range 0.5–0.9 eV), and a spectroscope in the visible to UV light region, Hamamatsu C10027-01 (Light detector; effective range 1.3–5 eV). Outputs of the two detectors are averaged radiation power of multiple measurements as a function of wavelength. The measurement time is about 30 seconds for Nr-IR and 50 seconds for

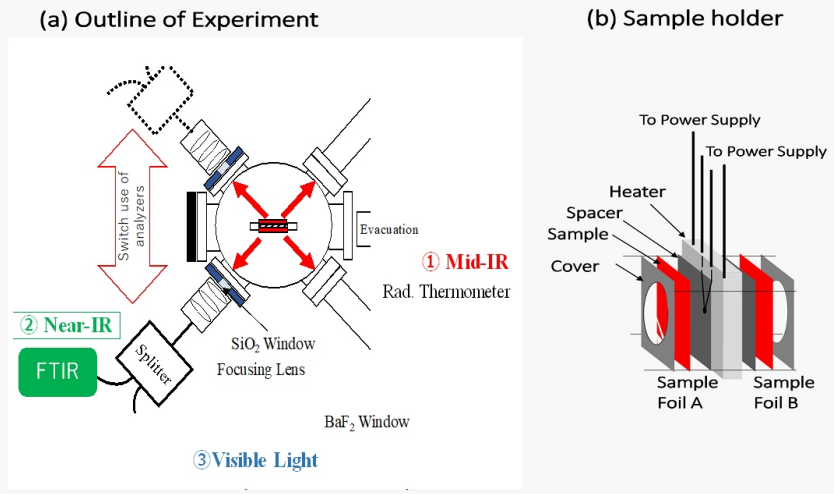

Figure 1. (a) Top view of experimental apparatus, showing inside of vacuum chamber. A sample holder with two foils of a sample placed in a vacuum chamber. Photon detectors are placed outside of the chamber. There are two sets of radiation thermometer in mid-infrared region (Md-IR), an FTIR spectrometer in near-infrared region (Nr-IR) and a multi-channel spectrometer in visible to UV light region (Light). (b) Sample holder. Two sample foils are placed on both sides of a ceramic heater and fixed with Photoveel covers. The ceramic heater has a built-in thermocouple in the center to measure temperature.

Light. It is also noted that measured photons are apertured to accept light only from the samples, not from the entire region including the sample holder.

2.2. Samples

Preparation of samples has been described in detail in [15], [16]. Measurements for the following four samples are shown in the present work. (1) pure Ni: 99.9% purity of Ni foil, 0.1-mm thick with area of 25×25 mm^2. (2) Ni5Cu1 sample: Layers of Cu (3.8-nm thick) and Ni (20-nm thick) are alternatively deposited by magnetron sputtering to form 6 bilayers on (1) Ni substrate. (3) Ni1Cu3 sample: Layers of Cu (17.8-nm thick) and Ni (6-nm thick) are alternatively deposited by magnetron sputtering to form 6 bilayers. (4) pure Cu: single layer of Cu (140 nm) is deposited on the Ni substrate.

2.3. Experimental Procedure

The measurement was performed for each sample with the following procedures.

(1) Sample baking: Foils A and B are placed in position in the chamber, which is evacuated down to a pressure of less than 3×10^{-6} Pa for a vacuum bake-out by keeping the heater temperature at about 1150 K. The bake-out lasts about 3 days.

(2) Measurement without H_2 gas: Keeping the inside of the chamber in a vacuum, set the voltage of the heater input (V_{in}) to a given value. Measure the radiant power spectra at about 0.5 h and 3 h after V_{in} is set. Set V_{in} to a different value and repeat the measurement for at least 5 different values of V_{in}. The results serve as a calibration with null excess energy.

(3) Measurement during desorption of H_2 gas: Fill the chamber with H_2 gas to 200–300 Pa and keep the temperature at about 520K so the sample absorbs gas. After 12 -15 h, evacuate the vacuum chamber at the same time as setting the value of V_{in}. Start the data logger and measure the radiant power spectra at about 0.5, 1.5, 4.0 and 6.0 hours after V_{in} is set. Repeat from the filling of H_2 gas for different values of V_{in} at least 4 times. The data will show the temperature dependence of the excess power together with elapsed time dependence for a short period.

(4) Long-term measurement without hydrogen refilling: For the NiCu sample, a long-term measurement is performed in order to see the long-term behavior of the excess power. After hydrogen absorption into the sample, the measurement with $V_{in} = 46$ V is started similarly as in (3) but the radiant power spectra are measured every 30 minutes for 5 consecutive days without refilling the H_2 gas.

During the above measurements, the data logger records the following information every second to monitor the experiments; heater temperature, output of Md-IR (mid-infrared thermometer), heater voltage and current, vacuum chamber pressure, chamber outer wall temperature.

3. Results and Discussion

3.1. Radiation Power Spectra

Photon emissions from foils A and B were measured separately as shown in Fig. 1. The two measured intensities were added together to give the average radiant power of the sample. Examples of such radiation spectra are shown in Fig. 2 for samples with different composition ratios. They correspond to the samples, pure Ni, Ni5Cu1, Ni1Cu3 and pure Cu, from left to right, respectively. Black x-marks are the data measured before H_2 gas introduced (without H_2), and red circles are those measured during H_2 gas desorption (with H_2). For each pair, the heater input voltage was set to the same value (or input power was almost equal), in order to directly observe the change in radiation power with and without hydrogen.

It is obvious that all samples show enhanced radiation power during H_2 desorption, i.e., with H_2: Samples with NiCu composite layer show largely enhanced with H_2 over without H_2, while those with mono-layer of Cu or Ni show slightly.

An important feature of the obtained spectra is that they can be well described by gray-body radiation. Red and black curves shown in Fig. 2 are the best-fit spectra calculated by gray-body approximation, in which the radiant power is expressed as

$$Y(E_{\rm ph}) = \varepsilon_s(\sigma/\pi)E_{\rm ph}^3/(\exp(E_{\rm ph}/{\rm kT}_S) - 1). \tag{1}$$

Here E_{ph} is the photon energy (eV), ε_s is the emissivity and T_S is the surface temperature, σ is the Stephan-Boltzmann constant, and *k* is the Boltzmann constant. Values of ε_s and T_S are determined so as to give a best fit curve to the data. Table 1 shows the deduced values of ε_s and T_S corresponding to the spectra shown in Fig. 2. In these examples, T_S increases after H_2 introduced, while ε_s decreases. An increase in temperature is a prerequisite for excess radiant power. The emissivity depends not only on the type of metal but also on the surface condition, and usually decreases mainly due to the reduction of the surface oxide layer by the introduction of H_2 gas.

As we will see below, a quantitative evaluation of the thermal power requires the total radiant power flow Q_S from the sample, that is deduced as

$$Q_S = 2\pi A_S \int_0^{\frac{\pi}{2}} \int_0^{\infty} Y\left(E_{\rm ph}\right) dE_{\rm ph} cos\theta sin\theta \; d\theta = A_S\varepsilon_s\sigma T_s^4, \tag{2}$$

where A_S is the emission area of the sample. Also, the ratio of ε_s with H_2 to without H_2 is required to determine the excess power. We define $\beta = <\varepsilon_s$ with H_2>/<ε_s without H_2> for each sample, where the numerator is the average value of ε_s with hydrogen and the denominator is the average value of ε_s without hydrogen.

Table 1. Sample temperature T_S (K) and emissivity ε_s deduced from radiation power spectra shown in Fig. 1. The last column shows the input power P_{in} (W) during the measurement.

	Ni pure with H_2/without H_2	Ni5Cu1 with H_2/without H_2	Ni1Cu3 with H_2/without H_2	Cu pure with H_2/without H_2
Ts (K)	1020 / 1009	971 / 926	1013 / 984	997 / 983
ε_s	0.114 / 0.116	0.143 / 0.155	0.132 / 0.137	0.179 / 0.180
Pin (W)*	34.8 / 35.2	34.2 / 35.0	25.9 / 26.2	28.2 / 28.3

*The large difference in heater power between the first two and the latter two is due to changes made to the sample holder to reduce its thermal capacity.

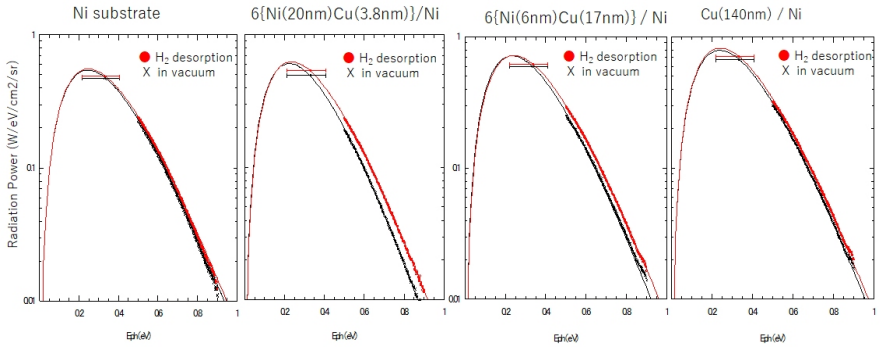

Figure 2. Examples of photon radiation spectra emitted from samples with different Ni/Cu ratio; pure Ni, Ni5Cu1, Ni1Cu3 and pure Cu, from left to right. Radiant power (W eV^{-1} cm^{-2} sr^{-1}) is plotted as a function of photon energy E_{ph} (eV). Red circles are the data measured during H_2 desorption, while x-marks are those without H_2 gas. For the lowest energy data, the point represents the averaged value within the horizontal bar. A solid line shows the best-fitting calculation with a gray-body radiation approximation.

3.2. Evaluation of Excess Heat

Figure 3 shows heat flow in the steady state: a simplified view (left side) and a model diagram used for the analysis (right side). There are two heat sources. One is the heater located between the sample A and B as indicated in Fig. 1(b), and the other is in the sample used to generate the excess heat. As shown in the diagram, the heat from the heater (P_{in}) transferred to the sample through the spacer and merges with the excess heat (Q_{ex}) in the sample. The sum of the heat (Q_{tot}) is almost all consumed as radiation to the chamber wall from the sample (Q_S) and the holder (Q_H). Contributions of the conducted heat flow (Q_C) through the supporting rod and the reflected radiation from the wall are very small (the latter is ignored in the analysis). Thus, relations between the heat flows and temperatures are expressed by the following equations.

$$\begin{aligned} Q_{\rm tot} &= P_{\rm in} + Q_{\rm ex} = Q_S + Q_H + Q_C, \\ Q_{S(H)} &= A_{S(H)}\varepsilon_{S(H)}\sigma T^4_{S(H)}, \\ T_C - T_S &= P_{\rm in}\, R_C, \\ T_S - T_H &= (P_{\rm in} + Q_{\rm ex})\, R_{\rm SH}, \\ T_H &= Q_C R_W, \end{aligned} \tag{3}$$

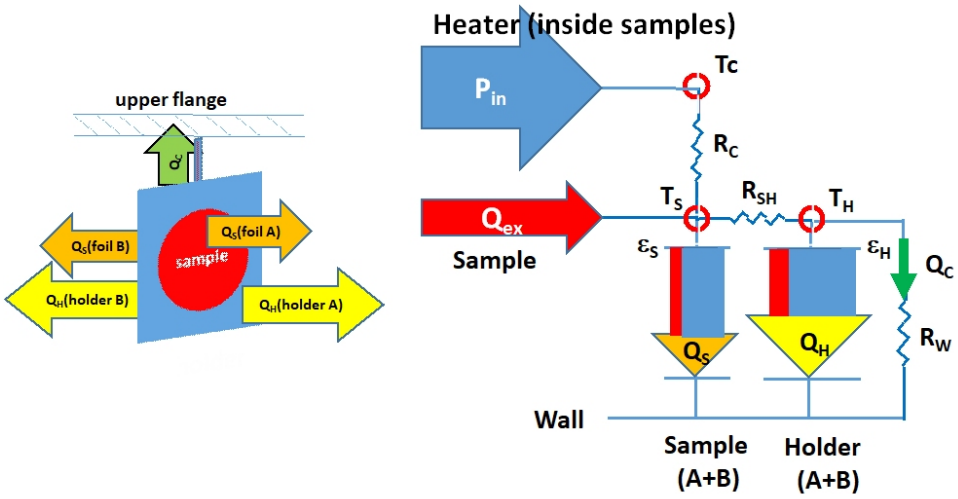

Figure 3. Heat flow diagram, schematic view (left side) and simplified heat flow model (right side). Arrows show heat flows. Heat flows from heat sources are colored gray for P_{in} (heat generated in heater) and red for Q_{ex} (excess heat generated in sample). Those of flowing out from the sample are orange for Q_s (radiation of sample), yellow for Q_H (radiation of holder) and green for Q_C (conduction through rods).

where $A_{S(H)}$, $\varepsilon_{S(H)}$ and $T_{S(H)}$ stand for the surface area, emissivity and temperature of the sample (holder), respectively, and σ is the Stefan-Boltzmann constant. R_C, $R_{\rm SH}$ and R_W are thermal resistances between the heater and the sample, the sample and the holder, and. the holder and the chamber wall, respectively.

Since both ε_S and ε_H little depend on temperature in this measurement, T_S and T_H determine the ratio Q_H/Q_S and, hence, it is described as $Q_{tot} - Q_C = (1 + Q_H/Q_S)\, Q_S$. If $R_{SH} = 0$, i.e., $T_H = T_S$, or $T_H = const \times T_S$, then the proportional relation $Q_{tot} - Q_C = \alpha\, Q_S$ holds strictly ($\because \alpha = 1 + \frac{\varepsilon_H}{\varepsilon_S}(\frac{A_H T_H^4}{A_S T_S^4})$). Even if it is not the case, the numerical simulation shows that linear approximation with $Q_{tot} - Q_C = \alpha\, Q_S + C$ is effective as long as $T_S/T_H \leq 1.2$ and $Q_S \geq 0.3$ W. Since the estimated value of T_H is about $T_S - 100$ at $T_S \approx 900$K, it is applicable to the present analysis.

However, after introduction of H_2 gas, the emissivity of the sample changes to ε'_S ($= \beta\, \varepsilon_S$), while thermal properties of Photoveel do not change with or without H_2; i.e., ε_H unchanged. In such a case, even when no excess power is generated, T_S increases to T_S' for $\beta < 1.0$. This causes an increase in T_H to T_H' also. But Q_S decreases to Q_S' ($Q_S = A_S \varepsilon_S \sigma T_S^4$ to $Q'_S = A_S \varepsilon'_S \sigma T_S'^4$) by the amount that Q_H increases to Q_H' ($Q_H = A_H \varepsilon_H \sigma T_H^4$ to $Q'_H = A_H \varepsilon_H \sigma T_H'^4$), since Q_{tot} stays constant. In other words, after hydrogen is introduced, the term Q_H/Q_S becomes Q_H'/Q_S' ($> Q_H/Q_S$) and the value of α determined before H_2 introduction should be corrected corresponding to this change. Using the approximation, $T_H' = const \times T_S'$, we replace α with $\alpha' = (\alpha + \beta - 1)/\beta$. Thus, the value of Q_{tot} must be evaluated by the following calibration equation.

$$Q_{tot} = P_{in} + Q_{ex} = \alpha' Q_S + Q_C + C, \tag{4}$$

where $\alpha' = (\alpha + \beta - 1)/\beta$ with $\beta = \varepsilon'_S/\varepsilon_S$.

Although the conductive heat flow Q_C is very small as around 0.13 W, we evaluate it as $Q_C = -3.71 \times 10^{-3} - 3.603 \times 10^{-5} T_C + 1.257 \times 10^{-7} T_C^2$, which was experimentally determined before the measurement.

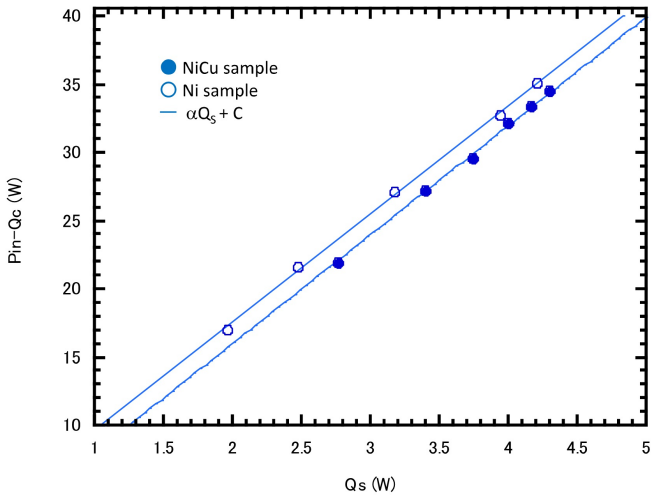

Figure 4. Calibration curves for pure Ni sample (open circles) and for Ni5Cu1 sample (closed circles). Data before H_2 gas introduction are plotted; Input power of the heater against deduced values of Qs.

Fig. 4 shows examples of calibration curves, $P_{in} - Q_C$ vs Q_S for Ni5Cu1 and pure Ni samples; they are measured for various P_{in} before the introduction of H_2 gas. Since no excess heat is expected without H_2 gas, we deduce values of α (corresponding to $\beta = 1$) and C by linearly fitting to the data. The solid blue circles are for the Ni5Cu1 sample and the open circles for the pure Ni sample. It is shown that the two data sets are very well fitted with respective straight lines. It should be noticed that the calibration curve is slightly different for each sample. This may be due to the individuality of the samples and subtle differences in the setting conditions.

The evaluation of Q_{ex} by the present calorimetry using measured Q_S and Eq. (4) may be more reliable than the conventional method that only uses heater temperature T_C. The following two points must be noted. (1) The effect of change in ε_s of the sample due to H_2 gas introduction should be taken in account: When ε_s decreases by 10% due to hydrogen introduction, T_S increases by about 2%, even without excess power generation. This results in an increase in T_C by similar amount. (2) The heat flow from the heater can be directly used as calibration for the present calorimetry: As shown in Fig. 3, the heat flow from the heater (P_{in}) determines the temperature difference ΔT between T_C and T_S and the temperature of T_S, but the heat flow (Q_{ex}) generated in the sample does not contribute to ΔT. Thus, it is not correct to use the relationship between T_C and P_{in} as a calibration curve, since this requires a situation that Q_{ex} originates at the heater position.

3.3. Quantitative Comparison of Excess Power

Applying Eq. (4), we have obtained the excess heat power Q_{ex}, shown in Fig. 5 as a function of the heater input power P_{in}; data of NiCu composite samples (Ni5Cu1 in left and Ni1Cu3 in right) are plotted by red solid circles, those pure Ni sample are plotted with red open circles in left, and those of pure Cu are plotted with orange closed circles. Data without H_2 used for the calibration curve are plotted with black x-marks. The error bar of each point corresponds to the random error (1σ), mostly originated from the error of Q_S, roughly 0.18% of its value. Two dashed lines, centered Q_{ex} = 0, show the systematic error (1σ) for Q_{ex}, being due to the uncertainty of the parameters of the calibration

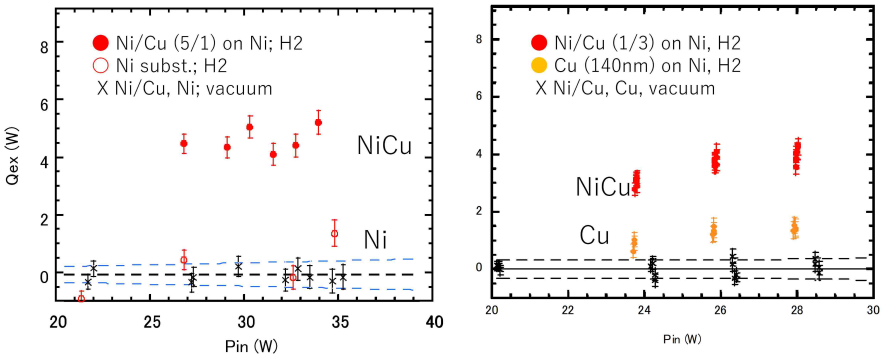

Figure 5. Excess heat power Qex (W) plotted against heater input Pin (W). Red solid circles are data for NiCu composite samples (Ni5Cu1 in left graph and Ni1Cu3 in right graph), red open circles are for Ni pure sample, orange solid circles for Cu pure sample, and x-marks for the data without H_2 gas. The error bar of each point corresponds to the random error (1σ), and the systematic error is indicated by two dashed lines, centered $Q_{ex} = 0$.

(α and C) and the ratio of the emissivity (β). It is shown clearly that the NiCu composite sample with H_2 produces large excess heat power; the amount is about 4–5 W and up to 17% of P_{in}. In contrast, the result of the pure Ni sample with H_2 is almost indistinguishable from those without H_2. The pure Cu sample produces Q_{ex} that is slight but can be measured with confidence. However, it is not certain that the excess energy source is in the Cu layer, since a possibility of alloying with Ni substrate cannot be ruled out. Using the thermal diffusion coefficient of Cu in Ni [18], all of the Cu on the surface is dissolved into the Ni substrate.

It is clear that the Ni/Cu binary thin film plays an important role in generating the large heat. However, the role of the initial layer structure may not be significant, since the layer structure may be lost thoroughly during the 3-day baking at about 1150 K before the measurement start. Measurements of the depth distribution of elements in samples after the excess heat measurement have been reported in [16] for composite thin films Ni/Cu and Ni/Cu/Y_2O_3. In the Ni/Cu sample, no traces of a layered structure were observed, while in the Ni/Cu/Y_2O_3 sample, decreasing wavy distribution of Y concentration was observed near the surface. The relationship between the magnitude of the generated heat power and the Ni/Cu ratio as well as the Ni/Cu structure remains to be addressed in the future.

3.4. Generated Energy

Figure 6 shows an example of long-term continuous measurement of Q_{ex}. The total energy generated in 80 hours is obtained by summing up the experimental values to be 460 $\pm$ 120 kJ. Since this is excess energy generated after H_2 is occluded in the sample, the energy source is considered to be a rection involving hydrogen in the sample. For the measurement of Fig. 6, hydrogen molecules of 6×10^{-6} moles were absorbed in the sample. Then, the amount of energy per H atom is 410 $\pm$ 108 keV/H atom, under the assumption that all H atoms are involved in the reaction. These huge amounts of energy that can never be produced from energy exchanges in electronic levels (chemical reactions). The actual amount of the produced energy per hydrogen atom should be much larger, considering the fact that most of hydrogen initially absorbed is quickly discharged into a vacuum by thermal diffusion, so it cannot participate in the reaction.

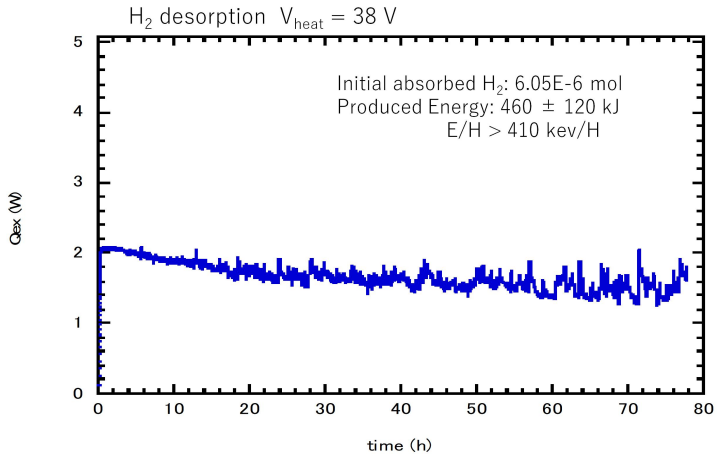

Figure 6. A result of 80-hour continuous measurement with two Mid-IR detectors for the Ni1Cu3 sample. Deduced excess heat power Q_{ex} (W) is plotted as a function of elapsed time (hour).

4. Conclusion

In studies of excess heat generation with NiCu multilayer thin film with H_2 gas, photon radiation calorimetry has been developed. Three types of photon detectors are employed in the measurement, giving a radiation intensity spectrum covering a wide range of photon energies from 0.2 to 1.8 eV. This serves as a means to compare the excess power produced in the sample, visibly although qualitatively. The spectrum is well approximated by gray-body radiation; the emissivity and temperature of the sample can be deduced. This is important, because a change in thermal properties may affect the evaluation of the excess power, especially at high temperature as in the present case (up to 1100 K). It is emphasized that the radiant calorimetry has advantages over thermometry.

By incorporating the measured radiation power into the heat flow model, we can evaluate the excess heat power quantitatively. It is emphasized that the calibration can be made correctly and the effect of change in emissivity can be taken into account. It was found that the sample having NiCu composite layer always produced larger excess heat than the pure Ni (or Cu) sample; the excess heat was deduced to be 4–6 W. The energy generated over 80 hours reached to 460 ± 120 kJ: the generated energy per hydrogen was at least 410 ± 108 keV/H atom. This is definitely not a chemical reaction. It produces energy at the level of nuclear reactions.

Acknowledgements

This work is supported by Clean Planet Inc., and The Thermal & Electric Energy Technology Foundation.

References

[1] M. Fleischmann and S. Pons, J. Electroanal. Chem. 261 (1989) 301.
[2] R.L. Mills and P. Kneizys, Fusion Technology 20 (1991) 65.
[3] R. Notoya, Fusion Technology 24 (1993) 202.
[4] G. Mengoli, et al., Nouvo Cimento 20D (1998) 331.
[5] S. Focardi, et al., Nouvo Cim. 111A (1998) 1233.
[6] A. Rossi, U.S. Patent 20110005506 A1, 2011.

[7] G. Levi, et al., arXiv 1305.3913 (2013)
[8] M. Valat, et al., J. Condensed Matter Nucl. Sci. 21 (2016) 81.
[9] K.P. Budko and A.I. Korshunov, J. Condensed Matter Nucl. Sci. 23 (2017) 85.
[10] C.P. Berlinguette, et al., Nature 570 (2019) 45.
[11] Y. Arata and Y.C. Zhang, J. High Temp. Soc. 34 (2008) 85.
[12] A. Kitamura, et al., Phys. Lett. A373 (2009) 3109.
[13] A. Kitamura, et al., J. Condensed Matter Nucl. Sci. 19 (2016) 135.
[14] A. Kitamura, et al., Int. J. of Hydrogen Energy 43 (2018) 16187.
[15] Y. Iwamura, et al., J. Condensed Matter Nucl. Sci. 29 (2019) 119.
[16] Y. Iwamura, et.al., J. Condensed Matter Nucl. Sci. 33 (2020) 1; ibid., 36 (2022) 285.
[17] T. Itoh et.al, J. Condensed Matter Nucl. Sci. 36 (2022) 274.
[18] H. Helfmeier and M. Feller-Knjepmeier, J. App. Phys. 41 (1970) 3202.